# Optimum Configuration of High-Lift Aeromaneuvering Orbital Transfer Vehicles in Viscous Flow

Carol B. Davies*
*Sterling Software, Palo Alto, California*
and
Chul Park†
*NASA Ames Research Center, Moffett Field, California*

**An aeroassisted transfer vehicle (AOTV) with a high lift-to-drag ratio ($L/D$) is appropriate for missions requiring a large plane inclination angle change. This paper compares the aerodynamic characteristics of three geometric configurations appropriate for such purposes and considers the need to protect and support the necessary payloads in the dead air region. The three configurations are the flat-plate delta wing, truncated straight cone, and truncated bent biconic. The analysis includes the effect of viscosity and examines the rounding of the sharp leading edges. Results indicate that, under the constraints of carrying a given volume in the dead air region, all three configurations provide similar values of $L/D$. However, the truncated bent biconic is the only configuration that provides the necessary stabilizing moments. Also shown is that a leading-edge bluntness with a radius of 0.1 m is easily tolerated for a body length of 35 m, with little degradation in $L/D$. An exception to this occurs for a high-aspect-ratio delta plate, where the same radius produces up to a 40% decrease in $L/D$.**

## Nomenclature

$A$ = frontal projected area
$C_d$ = drag coefficient, based on $A$
$C_f'$ = local skin friction coefficient
$C_l$ = lift coefficient, based on $A$
$C_{m_\alpha}$ = stability derivative
$C^*$ = Chapman-Rubesin constant, $(\mu/\mu_e)(T_e/T)$
$D$ = total drag
$F_n$ = normal pressure force on blunt leading edge
$f_t$ = accommodation coefficient
$L$ = total lift
$M$ = Mach number
$p_i$ = normal pressure force
$r$ = radius of blunt leading edge
$s$ = streamwise distance to leading edge, parallel to $x$-$y$ plane
$Re$ = Reynolds no. based on $s$
$V$ = velocity
$T$ = temperature
$(X_{c.g.}, Y_{c.g.})$ = center of gravity coordinate
$(X_{c.p.}, Y_{c.p.})$ = center of pressure coordinate
$\alpha$ = angle of attack with respect to reference axis
$\alpha_{min}$ = minimum angle of attack required to contain transport complex in dead-air region
$\alpha_q$ = equivalent angle of attack
$\beta_i$ = angle between local lift direction and $F_n$
$\gamma$ = stability parameter
$\delta_1$ = boundary layer displacement thickness
$\delta_2$ = boundary layer momentum thickness
$\lambda_i$ = angle between flow direction and cylinder axis
$\mu$ = viscosity
$\rho$ = density
$\tau_0$ = wall shear stress
$\phi_i$ = angle between flow direction and body normal

*Subscripts*

$i$ = general point on body surface
$\infty$ = free stream value
$e$ = boundary layer edge value

Presented as Paper 85-1059 at the AIAA 20th Thermophysics Conference, Williamsburg, VA, June 19-21, 1985; received May 27, 1986; revision received Dec. 19, 1986. 

*Consultant.
†Research Scientist. Member AIAA.

## Introduction

THIS paper describes the results of an analysis to determine the geometrical configuration of the aeromaneuvering orbital transfer vehicle that maximizes lift-to-drag ratio ($L/D$), while satisfying the constraints imposed on this type of entry vehicle. Three different configurations are analyzed: 1) flat-plate delta wing (delta plate), 2) truncated straight cone, and 3) truncated bent biconic. The first two configurations represent conventional concepts of hypersonic vehicle geometries, and we have previously proposed the third configuration as an alternative.[1] Several variations of these configurations are considered. Lift and drag of these configurations are determined by adding the inviscid Newtonian hypersonic values to those produced by the viscous friction forces. The viscous friction forces are calculated from the momentum equation for a two-dimensional laminar boundary layer.

An orbital transfer vehicle (OTV) is a type of flight vehicle proposed for the missions to transport payloads from one Earth-bound orbit to another.[2] There are two categories of missions expected for such vehicles: the altitude-change missions and the orbital-plane-inclination, angle-change missions.[2] In an altitude-change mission, the two orbits involved are at greatly different altitudes; in a plane-change mission, the two orbits are roughly at the same altitude, but they are in planes that are greatly different in their angles of inclination with respect to the Earth's equatorial plane.

The required velocity changes for these missions could be produced entirely by the use of rocket motors. With an aeroassisted orbital transfer vehicle (AOTV), some of the

velocity change can be accomplished by utilizing aerodynamic forces instead of rocket fuel. By passing through the atmosphere, deceleration or change in flight direction can be provided by the aerodynamic drag or lift forces produced on the vehicle. This will decrease the mass of the fuel to be carried and thus increase the payload capacity.

Two types of AOTVs have been considered to date: aerobraking and aeromaneuvering. An aerobraking vehicle is equipped with an aerobrake which produces relatively large drag but small lift. Mission scenarios, economic advantages, basic construction, and the expected performances of such aerobraking vehicles are well understood.[2-4] An aeromaneuvering vehicle has a lifting surface which produces large lift and small drag.[1,5] These vehicles are useful for missions that require large plane-inclinational changes. Flying at a high bank angle, such vehicles can turn laterally by utilizing lift forces. In order to produce a large-inclinational change, without losing much of the initial tangential flight velocity, a large $L/D$ is required. Mission scenarios and their economic advantages have been studied and show that an aeromaneuvering vehicle with an $L/D$ greater than 1.5 (preferably around 2.0) becomes advantageous over the aerobraking vehicle when large plane-inclinational changes are required.[6]

To date, the only significant aeromaneuvering vehicle configuration which has been proposed and studied is the bent biconic. The recent theoretical and experimental results indicate that the $L/D$ of this configuration will not exceed 1.5.[1,7] On the other hand, the concept of hypersonic airplane (or glideplane) has been in existence for many years. Such conventional concepts identify two basic types of configurations: flat-plate delta wing (delta plate) and truncated straight cone.[8] Recently, we proposed a truncated bent biconic as an alternative.[1] To date, no systematic comparison has been made of the relative merits of these configurations. It is the purpose of this work to compare the performances of these three configurations to arrive at the most desirable configuration. Several steps are taken to accomplish this:

1) Definition of physical and mission-oriented constraints, such as dimension, lift capability, and stability requirements.

2) Analytical generation of the body geometries with comparably sized lifting surfaces.

3) Computation of aerodynamic characteristics, such as lift and drag (including viscous effects), moments, and center of pressure. The latter is needed to determine stability parameters.

4) Introduction of a blunt leading edge.

5) Evaluation of the effect on the aerodynamic characteristics for varying body size, angle of attack, altitude, and blunt leading edge radius.

## Design Constraints

A typical AOTV configuration will consist of two major components: the component associated with the vehicle's transporting function, the transport complex, and the component that produces the aerodynamic forces and provides thermal protection of the transport complex, that is, the aeroassist structure. The transport complex must contain three modules: the propulsion, command/control, and payload modules. It is tacitly assumed that the complex will be constructed first and deployed to perform the payload delivery missions without the aeroassist structure and will be compatible with the dimensions of the Space Shuttle cargo bay, approximately 5 m in diameter and 15 m in length. The aeroassist structure supports the lifting surface and protects the transport complex stored in its dead-air region. Its overall shape and dimension must therefore be compatible with those of the transport complex. At the time of the AOTV entry, it is estimated that the mass of the transport complex will be about 5000 kg for delivery type missions and 10,000 kg for retrieval or abort missions.[5] This implies that the total lift of the vehicle must be sufficiently greater than 10,000 kg at the intended flight altitudes (60–90 km).[6] The vehicle also requires stabilizing pitching moments, and it would be advantageous for this stabilizing force to be entirely provided by the geometry of the vehicle.

## Body Geometries

The geometries of the three bodies are generated analytically by defining the normal at each surface point. The technique used to obtain the body coordinates of the truncated bent biconic is described in detail in Ref. 1. Briefly, the body shape is controlled by four variables; fore and aft half-cone angles, the bend angle between the two cone axes, and the proportion of the fore cone to the total body length. A fifth variable initiates a fourth-order polynomial which smooths the sharp transition edge between the two cones. Finally, the upper surface of the biconic is truncated by an arbitrary second-order curve that is tailored for the required cargo volume. This truncation will produce sharp leading edges; the effect of blunting these edges is also discussed in this report. The truncated cone is a special case of a truncated bent biconic with a truncation line almost parallel to the reference axis. The delta plate is the conventional shape that has a flat triangular lower surface. To fairly compare the characteristics of the different geometries the lifting surfaces are generated with equal areas. Figures 1a–1c show examples of the three configurations. In these figures, the upper portion shows the frontal view and the lower portion shows the side view. The reference axes indicate the line from which the angle of attack $\alpha$ is measured. In Fig. 1a, the term "cone angle" is used to indicate the sweep-back angle in order to maintain common terminology for all three configurations. The selected variables used to create the bent biconic shape seen in Fig. 1c (and subsequently used as the basic shape throughout this report) are a fore half-cone angle of 20 deg, an aft half-cone angle of 8 deg, and a bend angle of 2 deg. The variables describing the other two bodies were then generated to provide for equitable comparisons. Each body length is approximately 34 m with an under surface area of 300 $m^2$. Also shown for the truncated bodies is the frontal projection area $A$ (at $\alpha = 0$ deg) used as the reference area in the computation of drag and lift coefficients. The reference area of the delta plate is a function of the angle of attack. The force lines and center of pressure indicated in these figures are defined later in the section describing stability.

## Aerodynamic Characteristics

### Sharp Leading Edge

The aerodynamic characteristics of the three geometries are evaluated by considering each point on the body surface. Lift, drag, and moments will therefore be a function of the local body normal, the angle of attack, and the flight altitude. Lift and drag are calculated at each surface point by combining the inviscid flow values with those produced by wall friction and then summing them up over the entire lifting surface area. The lift ($C_l$) and drag ($C_d$) coefficients and $L/D$ are then evaluated.

The inviscid forces are calculated from the Newtonian hypersonic theory which describes the pressure at a local surface point as

$$p_i = \rho_\infty V_\infty^2 \cos^2 \phi_i \tag{1}$$

This pressure is then resolved into lift and drag directions.

The wall shear stress $\tau_0$ at $i$ is defined as

$$\tau_{0_i} = \tfrac{1}{2} C_f' \rho_e V_e^2 \tag{2}$$

All the boundary layer edge values were evaluated from the Rankine-Hugoniot relationship across an oblique shock wave. The shock angle is assumed to be 1.2 times the body angle at each surface point. This implies a specific heat ratio of approximately 1.4 in the hypersonic limit. Then, $\tau_{0_i}$ is resolved into lift and drag forces and added to the inviscid values. To

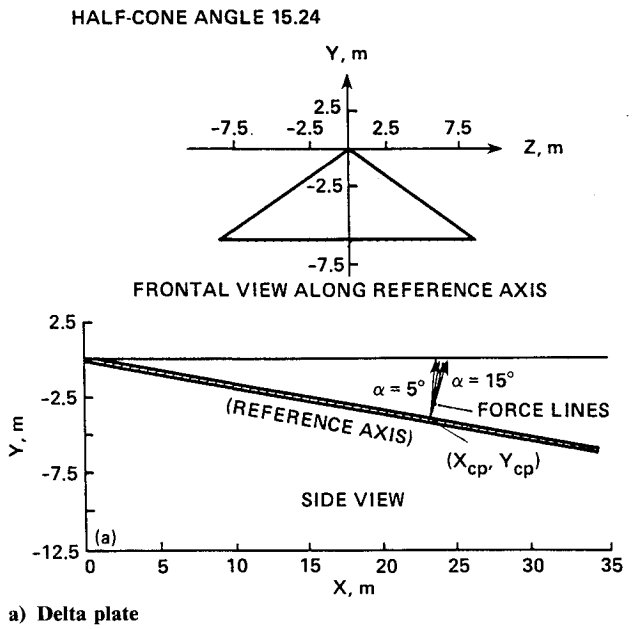


a) Delta plate

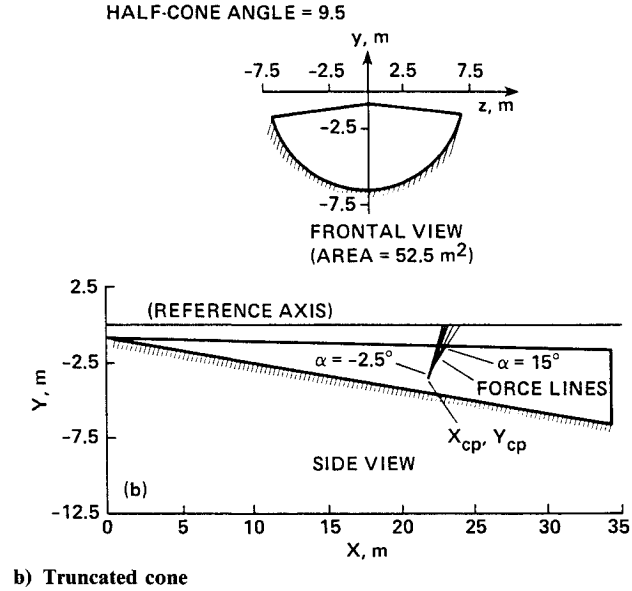


b) Truncated cone

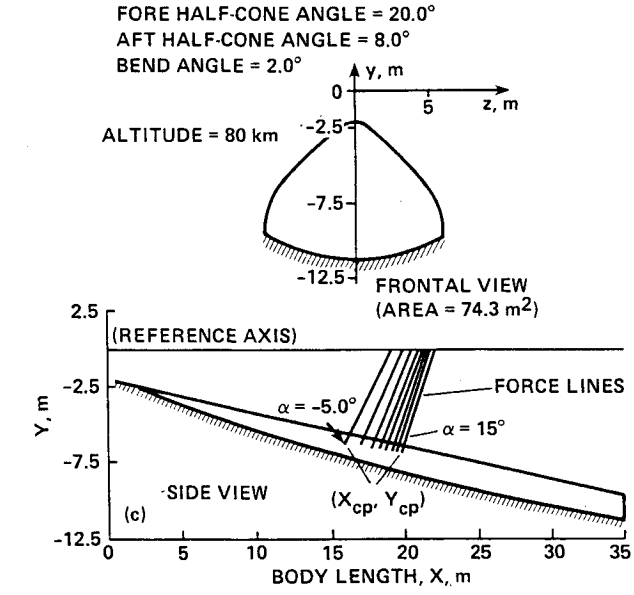


c) Truncated bent biconic

**Fig. 1 Side and front view of configurations.**

evaluate $C_f'$, the basic momentum equation for a two-dimensional laminar boundary layer is used to ensure that the effect of the curved surface of the truncated bent biconic and truncated cone is taken into account. This equation[9] is given by

$$\frac{\tau_0}{\rho}=\frac{1}{2}C_f'V^2=\frac{\mathrm{d}}{\mathrm{d}s}(V^2\delta_2)+\delta_1 V\frac{\mathrm{d}V}{\mathrm{d}s} \tag{3}$$

By expanding this equation and setting $\delta_1=2.59\,\delta_2$,[9] Eq. (3) simplifies to

$$C_f=2\frac{\mathrm{d}\delta_2}{\mathrm{d}s}+\frac{9.18}{V_e}\delta_2\frac{\mathrm{d}V_e}{\mathrm{d}s} \tag{4}$$

The first step is to solve for the growth rate of $\delta_2$. This requires knowledge of the flat-plate formula describing the local skin friction coefficient, which is a function of the flow conditions. A distinction is made between the strong interaction, weak interaction, and leading edge regions that are characteristic of rarefied hypersonic viscous flows.[10] For the leading-edge region, friction forces are calculated from the free molecular assumption, i.e.,

$$C_f'=0.664(f_t/M_e) \tag{5}$$

The flat-plate formula for the strong interaction[11] is given by

$$C_f=C_{f0}C_*^{1/4}\frac{M_e^{3/2}}{Re^{1/4}} \tag{6}$$

where $C_{f0}$ is a function that depends on the wall-to-stagnation temperature ratio. For a zero wall temperature $C_{f0}=0.208$.

The flat-plate formula for the weak interaction regime[12] is given by

$$C_f'=0.664\,(C_*^{1/2}/\sqrt{Re}) \tag{7}$$

Since Eq. (4) simplifies to $C_f'=2\mathrm{d}\delta_2/\mathrm{d}s$ for the flat-plate case, the appropriate skin friction formula can be used to find an autonomous form of $\mathrm{d}\delta_2/\mathrm{d}s$, which is substituted back into Eq. (4) and solved for $C_f'$. This solution for $C_f'$ depends on the flow regime around each surface point. The free molecular region spans such a small area that its influence on the overall characteristics is negligible. The delineation between the strong and weak interaction regimes is difficult to discern. In the more rarefied areas, the weak interaction formula yields a larger $C_f$ than that from the strong interaction formula.[12] To ensure no underestimation, both values were calculated at each surface point, and the largest was used to evaluate the viscous stress.

### Introduction of a Blunt Leading Edge

Up to this point, only sharp leading edges have been discussed. It is desirable to round these edges to minimize the high heat-transfer rates that will be encountered during atmospheric entry. A blunt leading edge produces an additional force that contributes to the aerodynamic characteristics. To simplify the geometry in the analysis, bluntness is provided by a circular cylinder superimposed along the contours of the leading edge for each configuration. The center of each small element of the cylinder coincides with the leading edge surface point used in the main body calculations. The inviscid lift, drag, and moments are evaluated for each elemental surface area and incorporated into the total body calculations. To obtain the lift and drag for a cyclindrical element, the normal force, $F_n$, on a cylinder of unit length is first computed. Application of the Newtonian theory leads to

$$F_n=4/3r\rho_\infty V_\infty^2\sin^2\lambda_i \tag{8}$$

The drag force acting on this unit cylinder is simply $D_i = F_n \cos\lambda_i$. The component of $F_n$ acting in the lift direction is $L = F_n \cos\beta_i$, where $\beta_i$ is the angle between $F_n$ and the lift direction. The lift and drag components are then multiplied by the elemental cylinder length and incorporated into the main body calculations.

#### Stability Parameters

The comparison of the stability characteristics of the three configurations is an important aspect of this work. An outline of the analysis for computing the stability parameters is presented here, but a more detailed description can be found in Ref. 1. For the vehicle to be stable at a particular angle of attack, a moment must be produced that will restore the body to the original angle of attack when a deviation occurs. The total lift moment is defined as the product of the local lift and the local lift moment arm summed up over the entire body surface. The total drag moment is obtained in a similar manner. The center of pressure ($X_{c.p.}$, $Y_{c.p.}$) is a function of the average length of the lift and drag moment arms. The location of this center of pressure is shown for each angle of attack in Figs. 1a–1c. For the delta plate and the truncated cone, it can be seen that the center of pressure remains fixed with varying angle of attack. However, for the truncated bent biconic, the location moves farther back as angle of attack increases.

The stability of these vehicles can be described by evaluating the conventional stability derivative $C_{m_\alpha}$ ($= dC_m/d\alpha$) where $C_m$ is the moment cofficient around the center of gravity ($X_{c.g.}, Y_{c.g.}$). Since the center of pressure and not the center of gravity is computed in the present analysis, a related variable called the stability parameter $\gamma$ is introduced. This parameter is defined as $(dX_{cp}/d\alpha)/X_L$, where $X_L$ is the body length. By assuming $Y_{c.p.} = Y_{c.g.}$, it can be shown that at the trim point, $\gamma$ is related to $C_{m_\alpha}$ by $\gamma = -C_{m_\alpha}/C_L$.

A body with a positive stability parameter (i.e., a negative stability derivative) provides stabilizing moments. Also shown in Fig. 1 are the force lines emanating from the center of pressure. These lines are the resultant of the total lift and drag forces that act at this point. The metacenter is defined as the intersection of the longitudinal axis and the resultant force line.

## Results and Comparisons

Figures 2a–2c show $L/D$ for the three configurations (without considering the restrictions on the cargo volume) over a wide range of angle of attack for altitudes ranging from 60–90 km. A freestream velocity of 9750 m/s is typical for an atmospheric entry from geosynchronous orbit, and this value was used in the calculations. It should be noted, however, that the results are almost insensitive to any anticipated range of freestream velocity. As expected, the highest $L/D$ for each configuration occurs at the maximum atmospheric density, i.e., at an altitude of 60 km. As altitude increases, the viscous effect also increases, producing a decrease in $L/D$.

The drag coefficient ($C_d$) of the truncated bent biconic was computed over the same range of angle of attack and altitude. At $\alpha = 0$ deg, $C_d$ increases from 0.14 to 0.18 between 60 and 80 km. but almost doubles at 90 km., indicating the greater effect of viscosity at the higher altitude.

Figures 3a–3c show the optimum placement of the transport complex within the dead-air region of the three configurations. The conditions to be satisfied for these placements are complex size (15 m × 5 m); position of the complex, to ensure that its center of volume coincides with the center of pressure of the aeroassist structure; and angle of attack, sufficient to maintain the complex within the dead-air region. In Fig. 3a, it is shown that the position of the complex within the delta plate remains fixed because of the fixed center of pressure. The $\alpha_{min}$ is defined as the minimum angle of attack required to maintain the complex within the dead-air region. The frontal view of the delta plate is also shown in this figure to indicate why $\alpha_{min} = 25$ deg. The $(L/D)_{\alpha_{min}}$ is defined as the value of the

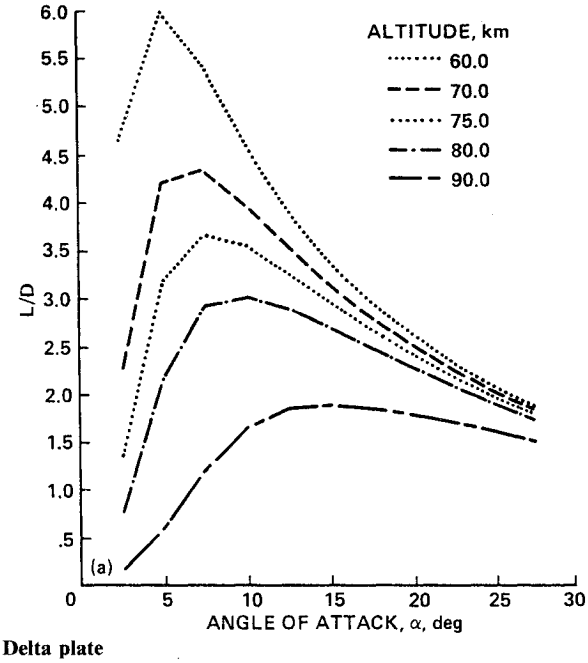


a) Delta plate

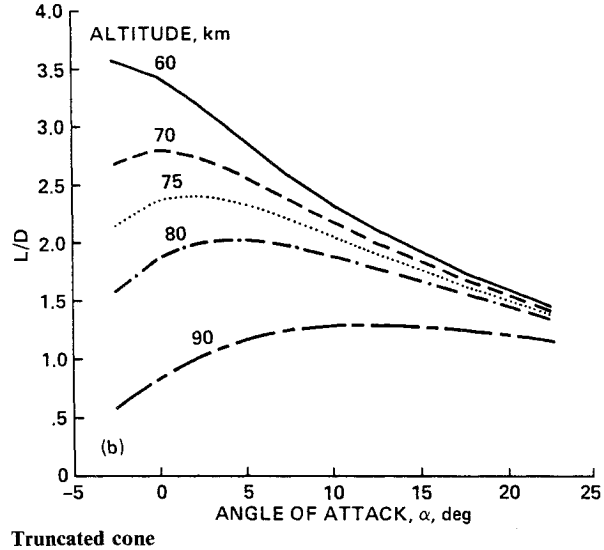


b) Truncated cone

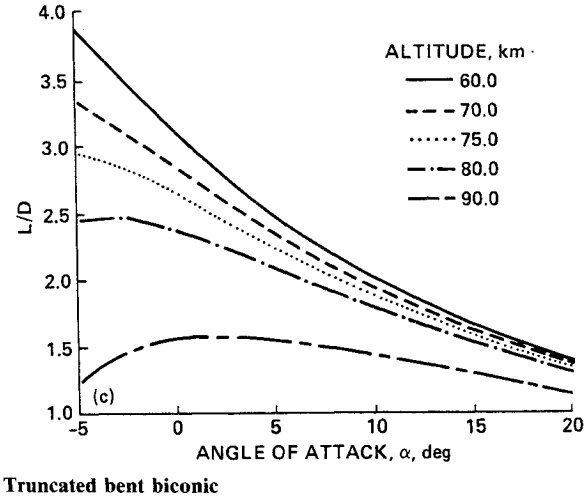


c) Truncated bent biconic

**Fig. 2 Change in $L/D$ with respect to angle of attack and altitude for sharp leading edges.**

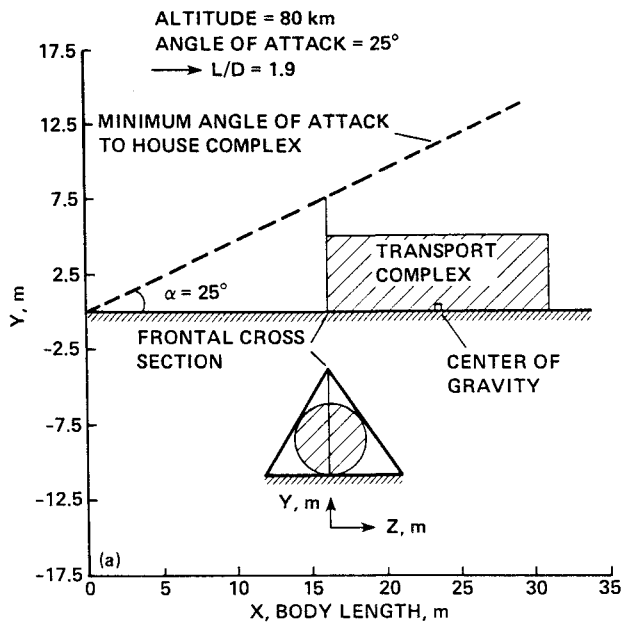


a) Delta plate

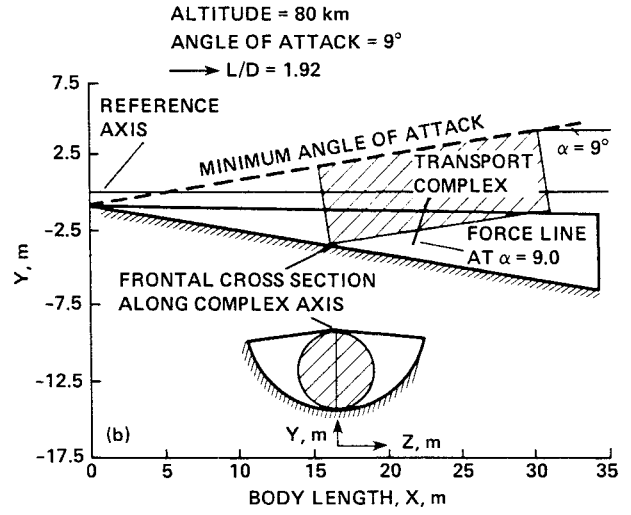


b) Truncated cone

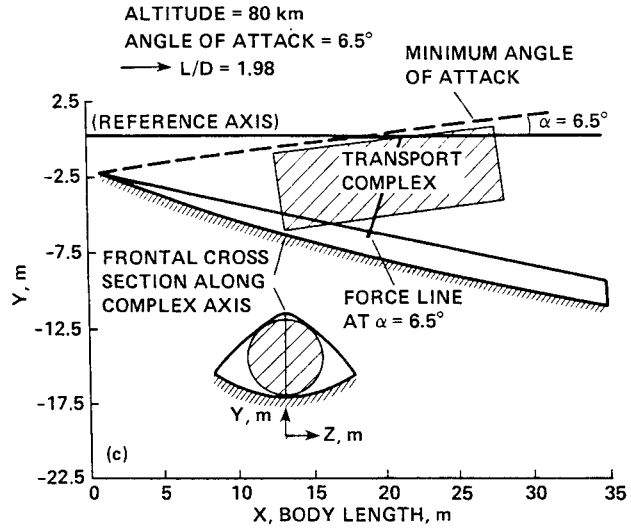


c) Truncated bent biconic

Fig. 3 Optimum placement of transport complex.

$L/D$ at $\alpha_{min}$ and, as seen in Fig. 2a, $(L/D)_{\alpha_{min}} = 1.9$ at an altitude of 80 km. In Figs. 3b and 3c, it can be seen that the transport complex fits more efficiently into the truncated geometries. The $\alpha_{min} = 9$ deg for the truncated cone and $(L/D)_{\alpha_{min}}$ is 1.92, which is very close to the maximum $L/D$ for this configuration. As in the case of the delta plate, the complex remains fixed around the constant center of pressure. For the truncated bent biconic $\alpha_{min} = 6.5$ deg and $(L/D)\alpha_{min}$ is 1.98.

Figure 4a compares $L/D$ for the three geometries at an altitude of 90 km and indicates the result of imposing the constraint of carrying the transport complex. To provide a more equitable comparison betweeen the body geometries, the

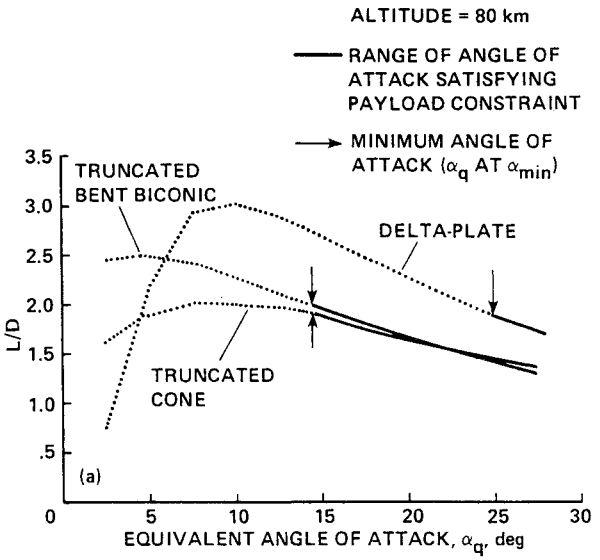


a) Viscous flow, including effect of payload constraints

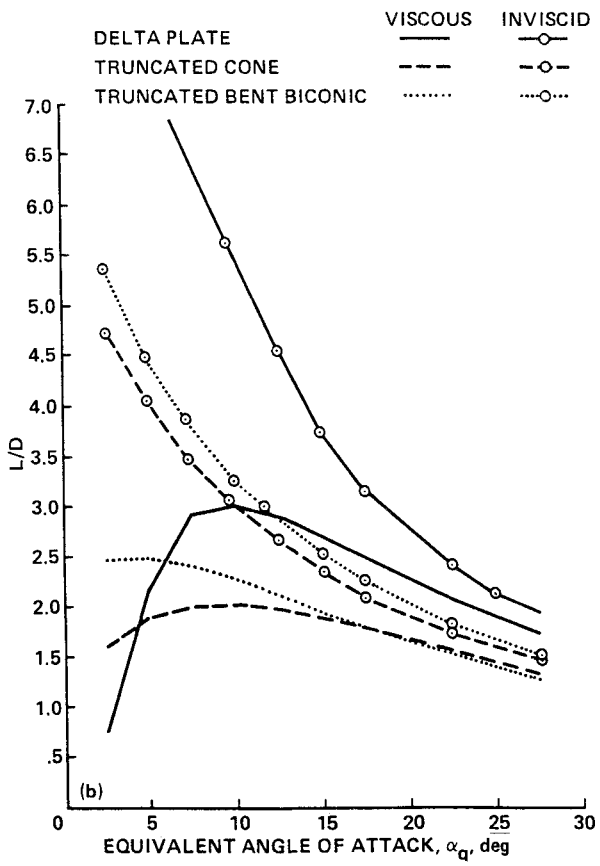


b) Comparison of viscous and inviscid $L/D$

Fig. 4 $L/D$ for the three configurations at 80 km.

equivalent angle of attack ($\alpha_q$) is used. This is defined with respect to the lower body surface of each vehicle and not the reference axis. This requires an average adjustment of 5 deg for the truncated cone and 7.5 deg for the truncated bent biconic. In the case of the delta plate, $\alpha = \alpha_q$. The maximum $L/D$ of 3.0 for the delta plate occurs at $\alpha_q = 10$ deg; $(L/D)_{max}$ for the truncated cone is 2.0 and also occurs at $\alpha_q = 10$ deg; and $(L/D)_{max}$ for the truncated bent biconic is 2.5 at $\alpha_q = 2.5$ deg. The $L/D$ decreases at the higher angles of attack with the values converging for the two truncated bodies. Although the full range of angle of attack is shown in this figure, the valid ranges of angle of attack (based on the values of $\alpha_q$ associated with $\alpha_{min}$) are indicated by the solid lines. It can be seen that any angle of attack greater than $\alpha_{min}$ lowers the value of $L/D$. It is significant to note that $(L/D)\alpha_{min}$ lies between 1.9 and 2.0 for all three configurations, thus producing a comparable $L/D$ performance at an altitude of 80 km. Figure 4b shows the same curves of $L/D$ but also superimposes the values of $L/D$ that are obtained when ignoring the viscous effects, i.e., when only Newtonian flow is considered. The viscous effects are very marked, dropping $L/D$ by 15 to 20%, at $\alpha_q$ greater than 20 deg, and by as much as 50 to 60% for the truncated bodies at the lower angles of attack. The $L/D$ for the delta plate is even more affected. The results shown in Fig. 4 represent an altitude of 80 km. To compare this with other altitudes, Fig. 5 plots $(L/D)\alpha_{min}$ against altitudes ranging from 60 to 90 km. All configurations show a rapid decrease in $(L/D)\alpha_{min}$ between 80 and 90 km. Although the delta plate has a lower $L/D$ at the lower altitudes, it is the most consistent over the full altitude range. The truncated cone exhibits the greatest range, with $(L/D)_{\alpha_{min}}$ dropping from 2.4 at 60 km to 1.27 at 90 km. The bent biconic, however, has the best overall $L/D$ performance.

Figure 6 shows total lift as a function of equivalent angle of attack. The configurations were generated with equal lower body surface areas. The calculations are shown for the 80-km flight altitude. From the figure, it can be seen that the total lift is sufficient at $\alpha_{min}$ for each geometry. At the higher altitude of 90 km, the situation is quite different: only the delta plate can maintain sufficient lift at its minimum angle of attack. The truncated bent biconic will have to fly at an angle of attack of 15 deg and the truncated cone at 27.5 deg.

To compare the stability of the three bodies, $\gamma$ is plotted vs an equivalent angle of attack. Figure 7 indiates the obvious difference between the truncated bent biconic and the other two configurations. The truncated cone and the delta plate have small, negative stability parameters. This is due to the almost constant (or slightly forward moving) location of the center of pressure with an increasing angle of attack. The truncated bent biconic has a large positive value, even at high angles of attack. This is created by the continual rearward movement of the center of pressure with respect to increasing angle of attack. This strong stabilizing characteristic of the truncated bent biconic is an important factor in determining suitable vehicle configurations for AOTVs.

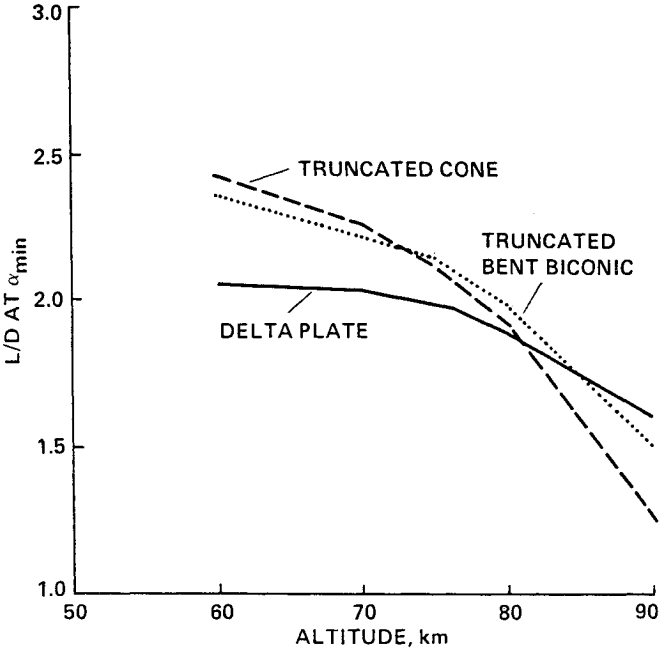


**Fig. 5 Change of $L/D$ with respect to altitude at optimum angle of attack for each configuration.**

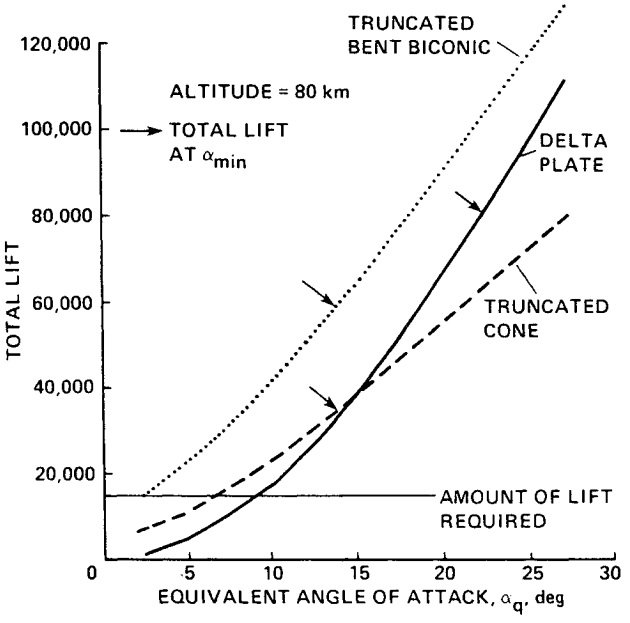


**Fig. 6 Total lift capability in kg for each configuration for a lifting surface of 300 m$^2$.**

### Blunt Leading Edge

The results presented so far represent configurations with sharp leading edges. To alleviate the high heat-transfer rates, it may be desirable to round these edges, thus causing some changes in the aerodynamic characteristics and stability of the configurations. The previous results were therefore reevaluated for configurations with blunt-edge radii $r$ from 0.1–1.0 m (i.e., from 0.3–3.0% of the total body length). A plot of $L/D$ vs $\alpha$ for various radii at an altitude of 80 km is shown in Fig. 8 for the truncated bent biconic. It can be seen that only a small decrease in $L/D$ occurs when $r = 0.1$ m, but the drop is more apparent with increasing radii. The same pattern occurs for the other two geometries. The effect of these increasing radii on the heat-transfer rates has been examined.[13] Results indicate that, for an altitude of 80 km, a radius of 0.1 m will reduce the convective heat-transfer rate by 50–75% of the value computed for the sharp leading edge. This percentage increases with decreasing altitude. Figure 9 shows the effect of altitude on the $L/D$ capability of the truncated bent biconic with an edge radius of 0.1 m. The curves for the other altitudes show the same slight drop in $L/D$. Calculations have also indicated the same pattern for the other two configurations. The values of the drag coefficient were also calculated and showed only a slight increase for $r = 0.1$ m, affecting $C_d$ at each altitude in the same proportion.

An interesting result was noted when evaluating the effect of bluntness on the stability parameter. Neither of the two truncated geometries showed any measurable change, but the delta plate now exhibits a positive stability parameter, i.e., the center of pressure moves back along the body as angle of attack increases. Figure 10 compares the stability parameter of the delta plate with a sharp leading edge to one that has a blunt

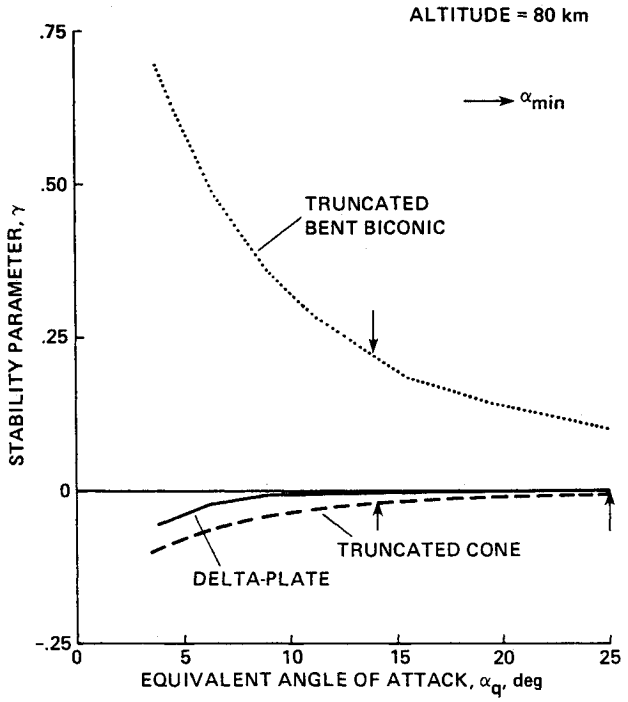


**Fig. 7 Stability parameter for each configuration.**

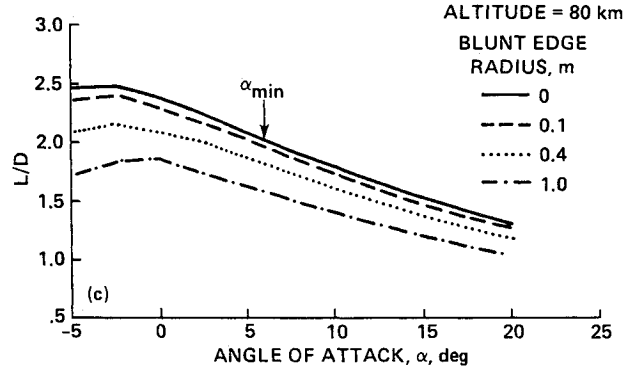


**Fig. 8 Effect on $L/D$ of increasing the blunt leading edge radius for the truncated bent biconic.**

leading edge of radius of 0.1 m. This change from an unstable to a more stable vehicle is due to the difference between the center of pressure of the cylinder to that of the delta plate. It should be noted, however, that this change is most noticeable for $\alpha < 10$ deg and at $\alpha_{min}$, the value of the stability parameter is extremely small and will have no practical application.

### Varying Body Dimensions

As previously stated, the geometries of these configurations are functions of body length and cone angles. The geometry of the truncated bent biconic configuration is also a function bend angle, cone juncture, and smoothing ability. In addition, the equation of the truncation line can vary for each of the truncated bodies. The body dimensions used in this report were determined by varying these descriptive parameters and choosing the set that provided a sufficiently high $L/D$ while minimizing the surface area (and thus the weight) of the aeroassist structure. The truncated bent biconic is described by several interdependent variables but it is felt that sufficient data sets were generated to provide descriptive parameters close to the optimum configuration. The effect of varying these parameters is described in the following, with a more detailed description given in Ref. 14.

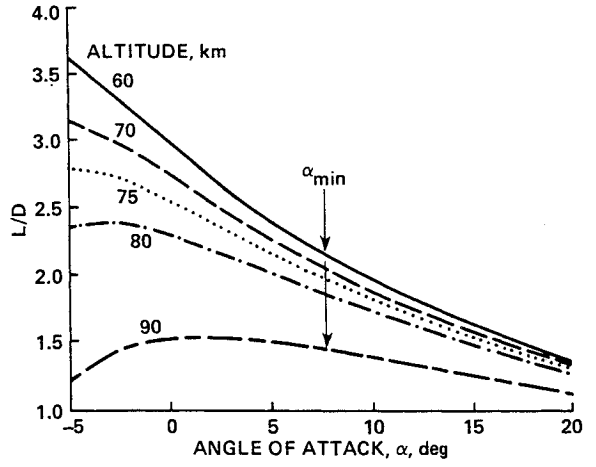


**Fig. 9 Effect of changing altitude on $L/D$ for the truncated bent biconic with blunt edge radius = 0.1 m.**

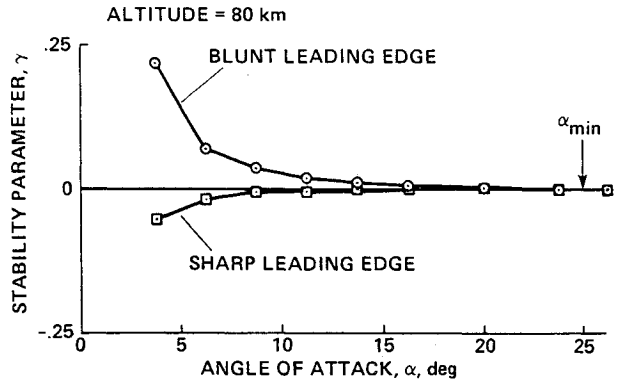


**Fig. 10 Comparison of stability parameters between blunt and sharp leading edges for delta plate.**

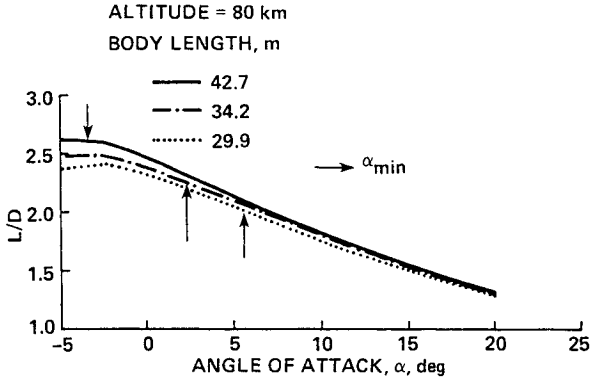


**Fig. 11 Effect on $L/D$ of changing body length for the truncated bent biconic.**

### Body Length

Figure 11 is a plot of $L/D$ vs $\alpha$ for truncated bent biconics of lengths 29.9, 34.2, and 42.7 m. The body length of 34.2 m has been used throughout this report. An important fact to note is that an increase in body length generates a much larger increase in surface area and therefore weight; however, this additional area does enable the transport complex to be more favorably positioned, thus producing an increase in $(L/D)_{\alpha_{min}}$. In these examples, $(L/D)_{\alpha_{min}}$ increases from 1.98-2.37 for the longer body and drops to 1.73 for the shorter length.

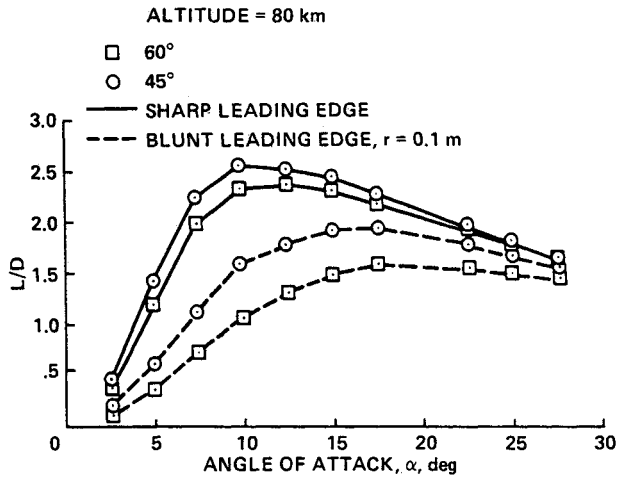


**Fig. 12 Effect of blunt leading edge on $L/D$ for high-aspect-ratio delta plate.**

Similar variations in length were made for the delta plate and the truncated cone. The changes in $L/D$ followed the same pattern as the truncted bent biconic, i.e., the longer body exhibits a slight increase and the shorter body exhibits a slight decrease in $(L/D)_{\alpha_{min}}$. In both these configurations, any finite decrease in body length proved to be impractical.

#### High-Aspect-Ratio Delta Plate

An increase in cone angle for the delta plate along with a decrease in body length will simulate a high-aspect-ratio vehicle. Fore cone angles of 45 and 60 deg were used to evaluate the aerodynamic characteristics for this type of configuration. The body lengths were adjusted to maintain the same surface area as the 34 m-delta plate that was analyzed previously. Figure 12 is a plot of $L/D$ vs $\alpha$ for both cone angles at an altitude of 80 km, and includes the effect of rounding the sharp leading edge. As seen in the figure, a blunt radius of 0.1 m produces a large decrease in $L/D$: for $\alpha < 15$ deg $L/D$ drops by more than 50%. This effect of the blunt leading edge is more significant than the change in cone angle. This result indicates that, for an AOTV, the addition of a delta wing, such as the kind used on the Space Shuttle, may prove to be disadvantageous. This type of wing with a high aspect ratio and blunt leading edge will produce relatively more drag than lift.

#### Truncated Cone

In this study the truncation line for the cone was almost parallel to the reference axis. This was chosen to represent a conventional vehicular shape, with consideration of yaw and roll stability. The truncated cone can be made considerably lighter, with no degradation in $(L/D)_{\alpha_{min}}$, by making the truncation equation similar to that used for the bent biconic. However, the stability parameter remains the same as that for the original body shape.

#### Truncated Bent Biconic

It is possible to generate many variations in the geometry of the bent biconic by changing its other descriptive parameters. One of these variables defines the proportion of each cone with respect to the total body length. Moving this juncture point toward or away from the nose will cause the center of pressure to move in the same direction, thereby repositioning the complex and causing a change in $\alpha_{min}$. At the same time, there is a small change in $L/D$; however, it is not sufficient to totally compensate for the change in $\alpha_{min}$, and the overall effect is a decrease in the $(L/D)_{\alpha_{min}}$. As mentioned earlier, the sharp juncture is smoothed by a fourth-order polynomial. Along with alleviating the physical problems encountered at sharp points, this smoothing also enhances $L/D$. In the bent biconic geometry, smoothing is initiated at the earliest opportunity.

## Conclusions

1) Throughout the full range of angle of attack and altitude considered in this report (without considering the placement of the transport complex), the delta plate exhibits the greatest range in $(L/D)_{max}$, varying from 1.8 at an altitude of 90 km to 6.0 at 60 km. For the truncated cone, the $(L/D)_{max}$ ranges from 1.25 at 90 km to 3.5 at 60 km. This can be improved by as much as 20% by varying the truncation line. At the same altitudes, the $(L/D)_{max}$ for the truncated bent biconic ranges from 1.55-3.9.

2) Positioning the complex within the dead-air region of the vehicles limits the maximum available $L/D$. At 80 km, the values of the $(L/D)_{max}$ are very close for each configuration: 1.98 for the truncated bent biconic, 1.92 for the truncated cone, and 1.9 for the delta plate.

3) The introduction of a small, blunt leading edge (e.g., a radius of 0.3% of the body length) only slightly affects each vehicle's aerodynamic performance, causing less than a 5% drop in $L/D$. Larger radii (e.g., 3.0% of body length) create a degradation in $L/D$ of up to 17% for the truncated bodies and up to 26% for the delta plate. In the special case of the high-aspect-ratio delta plate, this degradation can reach 40% for even the smallest radius considered.

4) Only the truncated bent biconic geometry provides stabilizing moments throughout the entire range of conditions investigated in this report. The truncated cone is always unstable, but the delta plate does provide small stabilizing moments when the leading edge is rounded.

5) A high-aspect-ratio wing, such as that used on the Space Shuttle, will significantly degrade the $L/D$ if used on an AOTV.

## References

[1]Davies, C.B. and Park, C., "Aerodynamic Characteristics of Generalized Bent Biconic Bodies for Aeroassisted Orbital Transfer Vehicles," *Journal of Spacecraft and Rockets,* Vol. 22, March-April 1985, pp. 104-111.

[2]Walberg, G.D., "A Survey of Aeroassisted Orbital Transfer," *Journal of Spacecraft and Rockets,* Vol. 22, Jan.-Feb. 1985, pp. 3-18.

[3]Scott, C.D., Reid, R.C., Maraia, R.J., Li, C.P., and Derry S.M., "An AOTV Aeroheating and Thermal Protection Study," *Progress in Astronautics and Aeronautics: Thermal Design of Aeroassisted Orbital Transfer Vehicles,* Vol. 96, edited by H.F. Nelson, AIAA, New York, 1985, pp. 309-337.

[4]Park, C., "A Survey of Aerobraking Orbital Transfer Vehicle Design Concepts," AIAA Paper 87-0514, Jan. 1987.

[5]Menees, G.P., Davies, C.B., Wilson, J.F., and Brown, K.G., "Aerothermodynamic Heating Analysis of Aerobraking and Aeromaneuvering Orbit-Transfer Vehicles," *Progress in Astronautics and Aeronautics: Thermal Design of Aeroassisted Orbital Transfer Vehicles,* Vol. 96, edited by H.F. Nelson, AIAA; New York, 1985, pp. 338-360.

[6]Menees, G.P., Brown, K.G., Wilson, J.F., and Davies, C.B., "Aerothermodynamic Heating and Performance Analysis of a High Lift Aeromaneuvering AOTV Concept," AIAA Paper 85-1060, June 1985; also, *Journal of Spacecraft and Rockets,* Vol. 24, May-June 1987, pp. 198-204.

[7]Miller, C.G., Blackstock, T.A., Helms, V.T., and Midden, R.E., "An Experimental Investigation of Control Surface Effectiveness and Real-Gas Simulation for Biconics," AIAA Paper 83-0213, Jan. 1983.

[8]Kim. B.S., Rasmussen, M.L., and Jischke, M.C., "Optimization of Waverider Configurations Generated from Axisymmetric Conical Flows," AIAA Paper 82-1299, Aug. 1982.

[9]Schlicting, H., *Bounday Layer Theory,* 6th Edition, McGraw-Hill, New York, 1968, p. 146.

[10]McCroskey, W.J., Bogdonoff, S.M., and McDougall, J.G., "An Experimental Model for the Sharp Flat Plate in Rarified Hypersonic Flow," *AIAA Journal,* Vol. 4, Sept. 1966, pp. 1580-1587.

[11]Boettcher, R.D., Koppenwaller, G., and Legge, H., "Flat-Plate Skin Friction in the Range between Hypersonic Continuum and Free Molecular Flow," *Rarified Gas Dynamics,* Vol. 51, Part 1, 1977, pp. 349-359.

[12]Wallace, J.E. and Burke, A.F., "An Experimental Study of Surface and Flow Field Effects in Hypersonic Low Density Flow over a Flat-Plate," *Rarified Gas Dynamics,* Supplement 3, Vol. 1, 1965, pp. 487-507.

[13]Brown, K.G., "Chemical and Thermal Non-Equilibrium Heat Transfer Analysis for Hypervelocity, Low Reynolds Number Flow," *Progress in Astronautics and Aeronautics: Thermophysical Aspects of Re-entry Flows,* Vol. 103, edited by J.N. Moss, AIAA, New York, 1986, pp. 445-477.

[14]Davies, C.B. and Park, C., "Optimum Configuration of High-Lift Aeromaneuvering Orbital Transfer Vehicles in Viscous Flow," AIAA Paper 85-1059, June 1985.